RESEARCH ARTICLE | DECEMBER 19 2023

Divergent interfacial thermal transport in MoS_2/Si heterostructure over optical phonon modes

Special Collection: Advances in Thermal Phonon Engineering and Thermal Management

Dongsheng Li ; Xiaona Huang; Zeyu Liu; Wenxiang Liu ; Shen Xu ; Yanan Yue

Appl. Phys. Lett. 123, 252201 (2023)
https://doi.org/10.1063/5.0180595

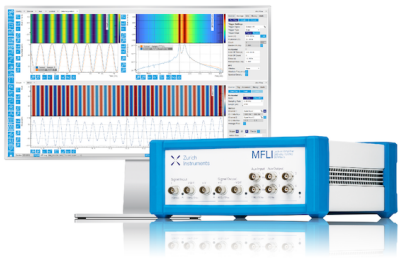

Applied Physics Letters ARTICLE pubs.aip.org/aip/apl

Divergent interfacial thermal transport in MoS_2/Si heterostructure over optical phonon modes

Cite as: Appl. Phys. Lett. **123**, 252201 (2023); doi: 10.1063/5.0180595
Submitted: 10 October 2023 · Accepted: 3 December 2023 ·
Published Online: 19 December 2023

View Online Export Citation CrossMark

Dongsheng Li,[1] Xiaona Huang,[1] Zeyu Liu,[2] Wenxiang Liu,[1] Shen Xu,[3] and Yanan Yue[1,a)]

AFFILIATIONS

[1]School of Power and Mechanical Engineering, Wuhan University, Wuhan, Hubei 430072, China
[2]School of Physics and Electronics, Hunan University, Changsha, Hunan 410082, China
[3]School of Mechanical and Automotive Engineering, Shanghai University of Engineering Science, Shanghai 201620, China

Note: This paper is part of the APL Special Collection on Advances in Thermal Phonon Engineering and Thermal Management.
[a)]**Author to whom correspondence should be addressed:** yyue@whu.edu.cn

ABSTRACT

Thermal transport within nanostructures is highly confined by interfaces, and non-trivial physics can emerge at boundaries. Theoretical studies have shown that different phonon modes can exhibit varying thermal resistances at interfaces. Experimental observation of these variations, however, is lacking. Using the steady-state Raman thermometry, the E^1_{2g} and A_{1g} vibrational modes of MoS_2 were utilized to characterize the thermal transport properties across the MoS_2/Si interface. Our results revealed distinct temperature rises associated with different modes, indicating various mode contributions in the interfacial thermal conductance. Combining experimental and numerical simulations, the out-of-plane mode in MoS_2 was found to contribute less to the interfacial transport, by 21.5%, attributed to the less variational mode mismatch of the in-plane phonon, compared to the in-plane mode. Furthermore, our results confirmed a 26.9% higher thermal conductivity from the out-of-plane mode than the in-plane one.

Molybdenum disulfide (MoS_2), a typical layered transition-metal dichalcogenides (TMDs), has high current on/off ration ($\sim 10^8$) and ultra-low standby power dissipation, ideal for advanced devices.[1–5] The MoS_2/Si interface becomes even more crucial, when integrating this novel Van der Waals material to existing Si-based electronics, especially for the optoelectronics applications.[6–8] However, with the lower dimension and higher integration density, more interfaces exist in those systems, impeding heat flow and causing heat accumulation in micro/nanostructured devices.[9,10] Managing heat flow across material interfaces and achieving fast heat dissipation has become one of the most important challenges in improving the performance and reliability of those devices.

Recently, various studies have shown the presence of phonon modes at the interface, which plays an important role in the interfacial thermal transport.[11–14] The in-plane modes are found to have a higher temperature rise than the out-of-plane phonon modes in the laser-irradiated single layer graphene using a computational approach.[15] Ruan *et al.* further found that different phonon modes may have different interface resistance, via molecular dynamics.[16,17] This will affect the temperature change sensed by the different modes and the corresponding interfacial thermal conductance. Overall, great progress has been made in the theoretical study of the effect of different phonon mode contribution on interfacial thermal transport. There is, however, still a lack of relevant experimental research and work as a major obstacle for understanding thermal transport in nanostructures.

Raman spectroscopy as a non-contact and fast characterization method can achieve atomic-level spatial and spectral resolution.[18,19] Based on the linear change between Raman shift and full width at half maximum of characteristic peaks with temperature, Raman thermometry is widely used in characterizing the interfacial thermal conductance and thermal conductivity of TMDs.[20–24] In addition, Raman spectroscopy can identify optical phonon patterns according to the atomic displacement of lattice vibrations. There are two prominent groups of Raman modes in MoS_2, the out-of-layer and the in-plane optical modes, related to the flexural optical phonon (ZO) and longitudinal/transverse optical phonon (LO/TO) modes, respectively.[19,25] Therefore, distinguish optical phonon mode contributions in thermal transport can be achieved by the different Raman modes.

In this work, the interfacial thermal transport properties of the MoS_2 film supported by the c-Si substrate within two different phonon modes were investigated by the Raman thermometry technique. MoS_2 has two prominent peaks in the Raman spectrum, which relate to the

in-plane (LO/TO) and out-of-plane (ZO) optical modes, respectively. The thermal response of two different phonon modes under two different laser heating spot sizes was investigated, and the temperature rise of phonon modes within different spot sizes was obtained. Full thermal transport properties of this heterostructure, including the interfacial thermal conductance and in-plane thermal conductivity within different phonon modes, were further determined based on the Raman thermometry and corresponding 3D finite volume simulation of laser heating. Phonon density of states (PDOS) are calculated to provide insights into the interfacial phonon transport mechanisms of the MoS_2/c-Si heterostructure. Those results further revealed the interfacial thermal transport properties under different phonon modes of the MoS_2 film supported on the c-Si substrate. In addition, this Raman laser irradiation experiment can further mimic the thermal management process in the MoS_2/Si photodetector, providing potential thermal constraints in the optoelectronics device design.

Figure 1(a) shows the schematic of the Raman experimental setup for the MoS_2/c-Si sample. Figure 1(b) shows the atomic structure of the typical layered MoS_2. The Mo atom is in the middle for each layer, and the distance between each layer is around 0.65 nm. In our experiment, the MoS_2 film was stripped by a micromechanical cleavage from bulk MoS_2 crystals and transferred to the c-Si substrate (supplementary material, Note 1). The thickness of the prepared MoS_2 film was around 9.2 nm (supplementary material, Fig. S1). Figure 1(c) shows the typical Raman spectra of the MoS_2/c-Si sample excited by 532 nm laser beam. The Raman spectra of the MoS_2 film have two predominated E^1_{2g} and A_{1g} Raman active modes surrounding 385 and 410 cm^{-1}, and the longitudinal optical phonon mode of c-Si nearing 522 cm^{-1}. The E^1_{2g} mode corresponds to the in-plane vibration of Mo and S atoms in the direction opposite to each other, which is related to the longitudinal/transverse optical phonon mode. The A_{1g} mode is associated with the out-of-plane optical vibration of S atoms, related to the flexural optical phonon mode.[26] Therefore, the Raman results from the E^1_{2g} and A_{1g} vibration modes are used to distinguish the contribution of the in-plane and out-of-plane optical mode in interfacial thermal transport.

While the MoS_2 film is excited by the Raman laser, the interfacial thermal conductance (G) and in-plane thermal conductivity (k_s) of the supported MoS_2 film satisfy the heat diffusion equation in the cylindrical coordinate,[27,28]

$$\frac{1}{r}\frac{d}{dr}\left(r\frac{dT}{dr}\right) - \frac{G}{k_S t}(T_M - T_a) + \frac{\dot{q}}{k_S} = 0, \quad (1)$$

where T_M is the temperature rise of the MoS_2 film upon laser heating, T_a is the temperature rise of the c-Si substrate, r is the radial position measured from the center of the laser beam, t is the thickness of the MoS_2 film, and $\dot{q}$ is the volumetric heating power. The G and k_S can be extracted based on the known average temperature rise for two different laser spot sizes (supplementary material, Note 4).

Based on the relationship between Raman shifts and sample temperature, the temperature under laser heating in Raman experiments can be determined. Thus, the calibration experiments of the MoS_2/c-Si sample at temperatures ranging from 296 to 382 K are first conducted. Figure 2(a) shows the eight temperature-dependent Raman spectra of the MoS_2/c-Si sample. The positions of the E^1_{2g} and A_{1g} modes are both red-shifted with increasing temperature, and it can be attributed to thermally driven bond softening.[29,30] In addition, the Raman peak near 522 cm^{-1} corresponds to silicon originating from the c-Si substrate. Similar red-shift with increasing temperature is observed. Figure 2(b) shows the temperature-dependent Lorentzian-fit peak frequencies for the E^1_{2g}, A_{1g}, and Si modes from the Raman spectra. The Raman peak position ω (in cm^{-1} units) shows a linear dependence with lattice temperature and can be expressed as follows[21] $\omega(T) = \omega_0 + \chi_T(T_\omega - T_0)$, where χ_T is the first-order temperature coefficient for the respective modes, and T is the absolute temperature. The extracted linear temperature coefficients χ_T from the slopes are −0.0135, −0.0131, and −0.0218 cm^{-1}/K for the E^1_{2g}, A_{1g}, and Si modes of the MoS_2/c-Si sample. The obtained temperature coefficient of the E^1_{2g}

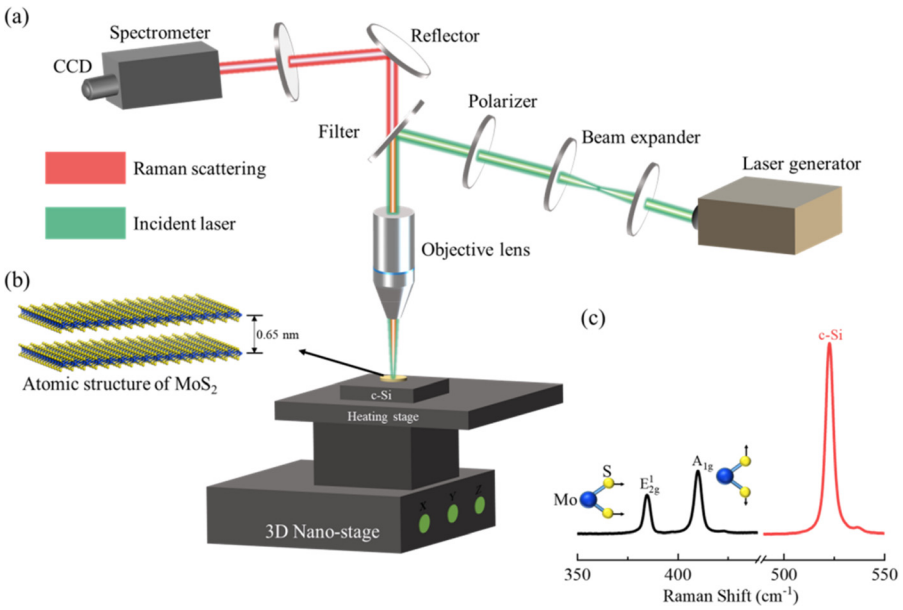

FIG. 1. (a) Schematic of the experimental setup for the micro-Raman experiment of MoS_2/c-Si sample. (b) The atomic structure of the MoS_2 film from a side view. The distance between two adjacent layers is around 0.65 nm. (c) Raman spectra of the MoS_2/c-Si sample are excited by the 532 nm laser and could be used to determine the temperature rise of the sample. The E^1_{2g} (385 cm^{-1}) and A_{1g} (410 cm^{-1}) modes of the MoS_2 and c-Si (522 cm^{-1}) LO phonon mode are observed in the sample.

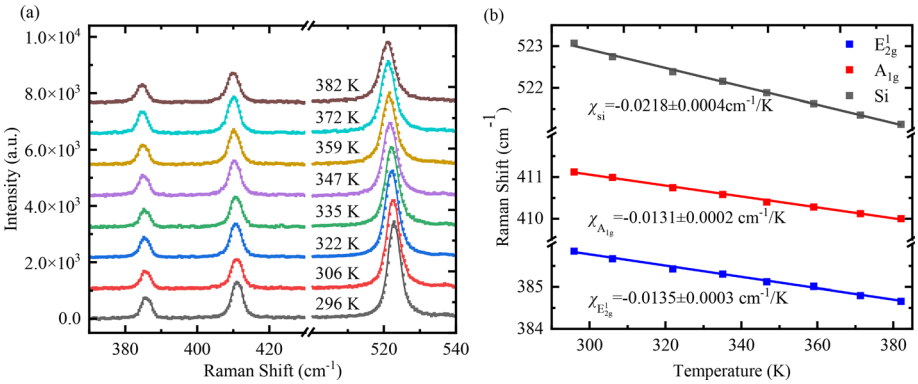

FIG. 2. (a) Raman spectra of the MoS_2 film and the c-Si substrate at an increased temperature during the Raman temperature coefficient calibration experiment. (b) The Raman shift for the E^1_{2g} and A_{1g} modes of MoS_2 and the c-Si substrate as a function of temperature in the calibration experiment. Fitting results for linear temperature coefficients are shown in the figure.

mode is very close to the A_{1g} mode, indicating that the temperature response of both phonon modes is not affected by interlayer interactions and the substrate.

To extract the relationship between the temperature rise of the MoS_2/c-Si sample with the laser power, the laser power-dependent Raman spectra were investigated. The power-dependent Raman spectra of the MoS_2/c-Si sample under 50× and 100× objective lenses are shown in Figs. 3(a) and 3(c). The intensity of the Raman peak under two objective lenses increases and red-shifts with laser power increasing. It can be attributed to the Raman-active mode softening due to local heating of MoS_2 as laser power increases. The Lorentzian-fit Raman peak position as a function of incident laser power is plotted in Figs. 3(b) and 3(d). The power-dependent peak positions can be characterized by a linear function,[21]

$$\Delta\omega = \chi_P(P_\omega - P_0) = \chi_P \Delta P, \tag{2}$$

where χ_P is the first-order power-dependent coefficient, and P is the incident laser power. Under 50× objective lens, the calculated χ_P is -0.0298 and $-0.0301\,\mathrm{cm}^{-1}$/mW for E^1_{2g} and A_{1g} modes, respectively. The values of χ_P show no significant difference between E^1_{2g} and A_{1g} modes, suggesting that both the in-plane transport and interlayer coupling dominate thermal transport. However, under 100× objective lens, the values of χ_P for E^1_{2g} and A_{1g} modes are -0.0930 and $-0.0875\,\mathrm{cm}^{-1}$/mW, respectively. The laser power coefficients for the

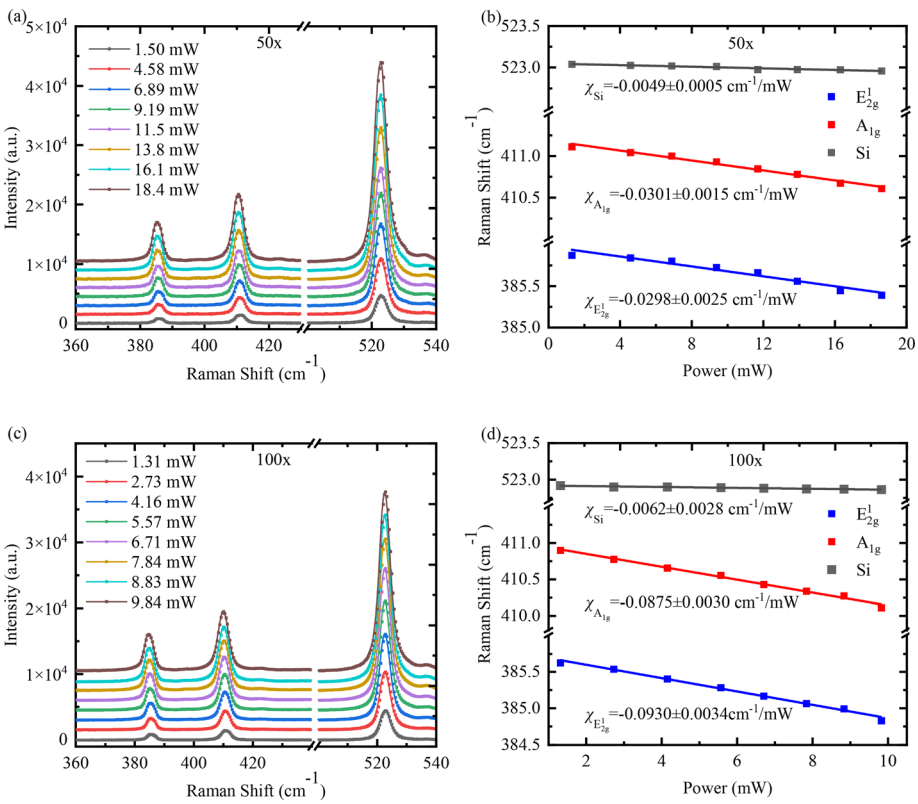

FIG. 3. Raman spectra of the MoS_2 film and the c-Si substrate at increased excitation laser power under (a) 50× and (c) 100× objectives in the ambient temperature. The Raman shift for E^1_{2g} and A_{1g} modes of MoS_2 and the c-Si substrate as a function of laser power under (b) 50× and (d) 100× objectives.

two vibration modes under 100× objective lens increase compared to those under 50× objective lens. The reason is that power density under 100× objective lens is higher, leading to more rapid temperature rise determined by Raman spectra. In addition, larger values of χ_P for the E^1_{2g} mode compared to the A_{1g} mode under 100× objective lens suggested that in-plane thermal transport is more sensitive and responsible for thermal transport with smaller laser spot sizes.

In the experiment, the red-shift of the Raman peak position was also observed in the Si modes of the MoS_2/c-Si sample, indicating that the substrate temperature rise was also caused by laser heating under the two different objective lenses. The average temperature rise per unit laser power of the MoS_2 film and c-Si substrate could be experimentally obtained by

$$\Delta\overline{T}_{MoS_2(c-Si)} = \frac{\chi_P}{\chi_T}. \quad (3)$$

Different temperature rise of the MoS_2 film and c-Si substrate can be obtained by 50× and 100× objective lenses, respectively. Here, the temperature difference between the MoS_2 film and c-Si substrate can be further obtained by $\Delta\overline{T} = \Delta\overline{T}_{MoS_2} - \Delta\overline{T}_{c-Si}$. Under the 50× objective lens, the calculated temperature differences are 2.02 and 2.21 K, corresponding to the E^1_{2g} (blue line) and A_{1g} (red line) modes, respectively. Under the 100× objective lens, the calculated temperature differences are 6.61 and 6.36 K, which correspond to the E^1_{2g} and A_{1g} modes, respectively.

To determine the G and k_s of the MoS_2 film supported on the c-Si substrate, a 3D numerical modeling based on the finite volume method was conducted to determine the temperature rise. The actual size and thickness of the MoS_2 film were applied in the 3D model as in the experiment. The cross-plane thermal conductivity of MoS_2 was taken at 2 W/mK,[31] and the thermal conductivity of c-Si was 148 W/mK. The incident laser power was 1 mW, and the laser spot size was identical to the experiment. In addition, the laser beam was incident vertically on the surface of MoS_2/c-Si, and the multiple reflection at the interface between MoS_2 and c-Si was considered, as shown in Fig. 4(a). According to the optical properties of MoS_2 and c-Si, based on the transfer matrix method (TMM),[32,33] the transmitted power at the top surface, the reflected power at the bottom surface of the MoS_2 film, and the transmitted power in the top surface of the c-Si substrate can be determined.

In the modeling process, a series of temperature differences between the MoS_2 film and c-Si substrate under laser heating focused with two different objectives was calculated with a different combination of the G and k_S. As mentioned earlier, the measured temperature rise of the MoS_2 film and c-Si substrate are the Raman-intensity weighted average temperature rise of the MoS_2/c-Si sample. The penetration depth of the Raman laser can be calculated by $\tau = \lambda/(4\pi\kappa)$, where λ is the laser wavelength, κ is the extinction coefficient of the sample under this laser wavelength. For the MoS_2 film, the extinction coefficient value is 5.2, and the calculated penetration depth is 38.5 nm. For the c-Si substrate, similar to the MoS_2 film, the temperature rise is an average temperature rise within the focal depth of the Raman probe laser. At 532 nm laser wavelength, the extinction coefficient value of c-Si is 1.1, and the calculated penetration depth is 820 nm. Thus, the temperature rise of the MoS_2 film and c-Si

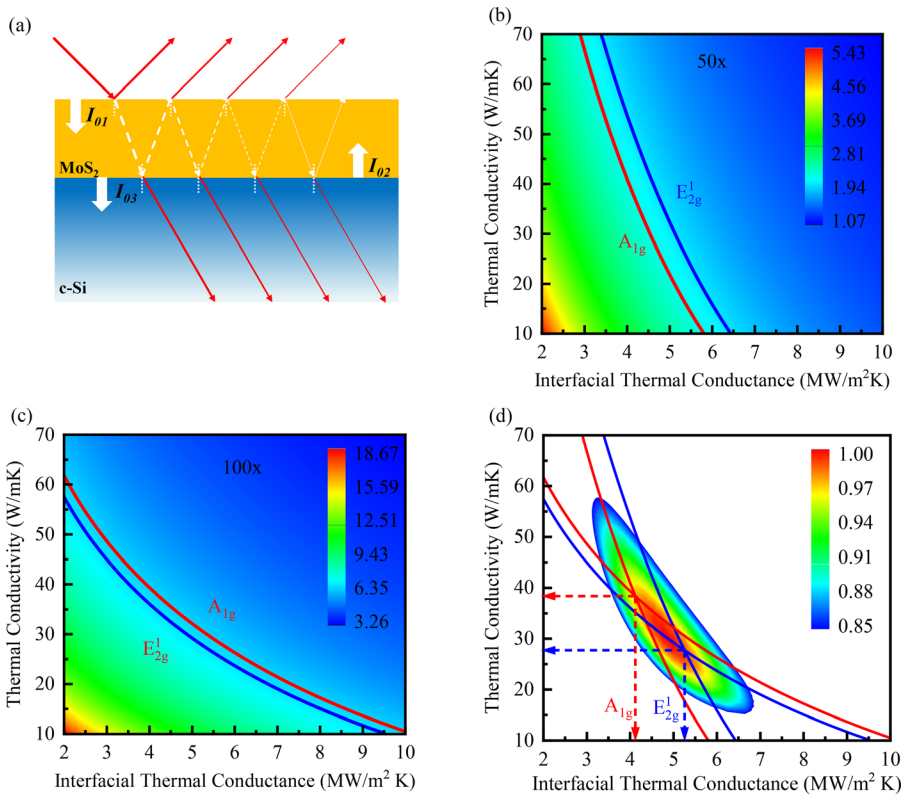

FIG. 4. (a) Schematic of the laser transmission. When the laser beam irradiates the sample surface, multiple reflections happen at the interface between the MoS_2 film and the c-Si substrate. The I_{01}, I_{02}, and I_{03} are the transmitted power at the top surface, the reflected power at the bottom surface of the MoS_2 film and the transmitted power in the c-Si top surface, respectively. The Raman intensity-weighted average temperature difference for a serious G and k_S is shown in (b) under 50× objective and in (c) under 100× objective lens. (d) Determined G and k_S by using E^1_{2g} and A_{1g} modes as well as the uncertainty region. The normalized probability distribution function contour shows the uncertainty distribution.

substrate can be calculated by $\Delta\overline{T} = \iiint \Delta\overline{T}_{MoS_2(c-Si)} I_{Raman} dV / \iiint I_{Raman} dV$. Among them, if the calculated temperature difference simultaneously agrees with the 50× and 100× experimental results, the corresponding pair of G and k_S is taken as the true properties of the MoS_2/c-Si sample. The calculated average temperature difference between the MoS_2 film and c-Si substrate under the 50× and 100× objective lenses in a series of G and k_S space are shown in Figs. 4(b) and 4(c). In both heating spot sizes, the lower k_S or G lends to a higher temperature rise. When k_S is lower, the heat of the laser heating region is difficult to diffuse laterally, leading to a higher local temperature rise and temperature difference between the MoS_2 film and c-Si substrate. When G is lower, achieving the same heat from the MoS_2 film to the c-Si substrate as that at the higher k_S requires a higher local temperature rise. In addition, under the 50× objective lens, the effects of G are more sensitive to the average temperature rise, which can be observed from the trend of the two isotherms. However, the effects of k_S on the average temperature rise is more significant for experiments using the 100× objective lens, especially at the lower value of G. This confirms the power-dependent coefficient difference between the E^1_{2g} and A_{1g} modes at 50× and 100× objective lenses.

For each laser heated spot size, the experimentally obtained temperature difference between the MoS_2 film and c-Si substrate (the isolines) could be satisfied by many different combined values of G and k_S. Thus, the results from both cases and normalized probability distribution function (Ω) can be used to determine the actual G and k_S in our experiments. Ω is defined as $\Omega = \exp[-(x-\overline{x})^2/(2\sigma^2)]$, where x, $\overline{x}$, and σ are the corresponding variable temperature difference, its average, and standard deviation, respectively. As shown in Fig. 4(d), a composite probability distribution function is defined as $\Omega_{(G,k_S)} = \Omega_{\Delta\overline{T}_{50x}} \cdot \Omega_{\Delta\overline{T}_{100x}}$ in the G and k_S space. The value of G and k_S is determined by the cross point of the 50× and 100× dashed curves. To show the results with uncertainty, the value of $\Omega_{(G,k_S)} = 0.6065$ corresponding to the σ probability is used to show the uncertainty of the final results. Finally, the obtained G by E^1_{2g} and A_{1g} modes are $5.26^{+1.27}_{-0.75}$ and $4.13^{+1.46}_{-0.96}$ MW/m^{2}K, respectively. The G obtained by the out-of-plane optical phonon mode is 21.5% lower than that obtained by the in-plane optical phonon mode; a similar phenomenon was also observed in the MoS_2/quartz interface.[34] It can be attributed to different acoustic phonon branches having different interface resistance, which results in a difference in the temperature rise and the measured G between the E^1_{2g} and A_{1g} modes.[16] Our results further indicated that for the 2D materials supported on the substrate, the in-plane phonon mode has better cross-interface thermal transport properties.

Phonon density of states (PDOS) are calculated to provide insights into the interfacial phonon transport mechanisms of the MoS_2/c-Si heterostructure, as depicted in Fig. 5. The obtained results are consistent with prior studies on MoS_2 and c-Si, showing similar peak positions.[35,36] A higher PDOS indicates a greater number of possible phonons at a given frequency. In the case of c-Si, the total PDOS at 385 cm^{-1} is higher compared to that at 410 cm^{-1} [Fig. 5(b)]. Consequently, more Si phonon modes exist at the E^1_{2g} mode of MoS_2, and less phonon mismatch is formed at the MoS_2/c-Si interface compared to the A_{1g} mode. We further decompose the PDOS of the Si substrate into in-plane and out-of-plane vibrations, as shown in Figs. 5(c) and 5(d). Similarly, more Si phonon in-plane vibration modes exist at the

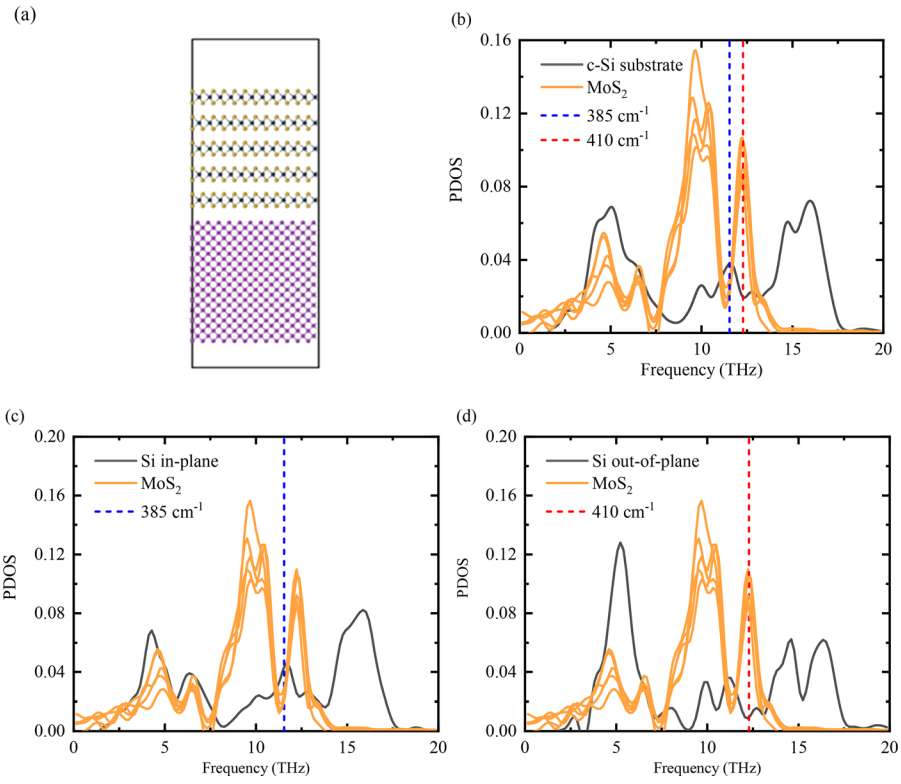

FIG. 5. (a) Schematic diagram of the MoS_2/c-Si heterostructure. (b) Phonon density of states of MoS_2 and the c-Si substrate. Phonon density of states of MoS_2 and the c-Si substrate from (c) in-plane vibrations and (d) out-of-plane vibrations.

E^1_{2g} mode of MoS_2 compared to the out-of-plane vibration modes at the A_{1g} mode. Thus, the former shows less phonon mismatch, resulting in a higher interfacial thermal conductance between the MoS_2 film and Si substrate. It should be noted that this mismatch in PDOS plays a crucial role in interfacial thermal transport, as demonstrated in precious research, and the mismatch results in a high thermal boundary resistance for the graphite/graphene-Cu_2Se interfaces,[37] the SiC-GaN interfaces,[38] and the Al–sapphire interfaces.[39] Thus, our experimental results of the 21.5% lower interfacial thermal conductance from out-of-plane optical mode than in-plane optical mode, which can be attributed to a lower mismatch in PDOS at E^1_{2g} mode of MoS_2. In addition, the calculated k_S by A_{1g} is $38.2^{+5.2}_{-6.2}$ W/mK, which is higher than the $27.6^{+5.4}_{-4.6}$ W/mK calculated by the E^1_{2g} mode. It can be attributed to the fact that the ZO mode was coupled strongly with the substrate for the in-plane thermal transport, which does not contribute much to the vertical thermal transport.[16,40,41] Those results further indicate the existence of different thermal transport properties among the phonon modes.

In summary, the interfacial thermal transport properties of the MoS_2 film supported on the c-Si substrate within two different phonon modes were investigated by the steady-state Raman method. Both the E^1_{2g} and A_{1g} modes of the MoS_2 film soften linearly as the temperature increases, with first-order linear coefficients of 0.0135 and 0.0131 cm^{-1}/K, respectively. By studying the thermal response of the MoS_2/c-Si sample under two different laser heated spot sizes and combining a 3D simulation, the interfacial thermal conductance G and in-plane thermal conductivity k_S of each mode were determined. The extracted G using the A_{1g} mode is 4.13 MW/m^2 K, 21.5% lower than the E^1_{2g} mode of 5.26 MW/m^2 K. In addition, the thermal transport difference between the two phonon modes is also reflected in k_S. The k_S calculated using the E^1_{2g} and A_{1g} modes are 27.6 and 38.2 W/mK, respectively. The calculated result of PDOS shows that the E^1_{2g} mode has a less phonon mismatch at the MoS_2/c-Si interface compared to the A_{1g} mode, leading to a high interfacial thermal transport property. These results indicate that the influence of different phonon modes of 2D materials' thermal transport cannot be ignored, further deepening the understanding of thermal transport characteristics in substrate-supported two-dimensional materials.

See the supplementary material for the experimental section and corresponding figures.

This study was financially supported by the National Key Research and Development Program of China (No. 2019YFE0119900), the National Natural Science Foundation of China (No. 52076156), and the Fundamental Research Funds for the Central Universities (No. 2042022kf1020). The authors appreciate the support from the Supercomputing Center of Wuhan University.

AUTHOR DECLARATIONS

Conflict of Interest

The authors have no conflicts to disclose.

Author Contributions

D.L., X.H., and Z.L. contributed equally to this paper.

Dongsheng Li: Conceptualization (lead); Data curation (lead); Formal analysis (lead); Methodology (lead); Writing – original draft (lead). **Xiaona Huang:** Formal analysis (equal); Investigation (lead); Methodology (equal); Writing – review & editing (lead). **Zeyu Liu:** Formal analysis (equal); Methodology (equal); Writing – review & editing (equal). **Wenxiang Liu:** Formal analysis (equal); Visualization (equal). **Shen Xu:** Formal analysis (equal); Validation (equal). **Yanan Yue:** Conceptualization (lead); Funding acquisition (lead); Supervision (lead); Writing – review & editing (equal).

DATA AVAILABILITY

The data that support the findings of this study are available from the corresponding author upon reasonable request.

REFERENCES

[1]H. Wang, L. L. Yu, Y. H. Lee, Y. M. Shi, A. Hsu, M. L. Chin, L. J. Li, M. Dubey, J. Kong, and T. Palacios, "Integrated circuits based on bilayer MoS_2 transistors," Nano Lett. **12**(9), 4674–4680 (2012).
[2]B. Radisavljevic, A. Radenovic, J. Brivio, V. Giacometti, and A. Kis, "Single-layer MoS_2 transistors," Nat. Nanotechnol. **6**(3), 147–150 (2011).
[3]Y. Liu, X. D. Duan, H. J. Shin, S. Park, Y. Huang, and X. F. Duan, "Promises and prospects of two-dimensional transistors," Nature **591**(7848), 43–53 (2021).
[4]N. Li, Q. Q. Wang, C. Shen, Z. Wei, H. Yu, J. Zhao, X. B. Lu, G. L. Wang, C. L. He, L. Xie, J. Q. Zhu, L. J. Du, R. Yang, D. X. Shi, and G. Y. Zhang, "Large-scale flexible and transparent electronics based on monolayer molybdenum disulfide field-effect transistors," Nat. Electron. **3**(11), 711–717 (2020).
[5]S. B. Desai, S. R. Madhvapathy, A. B. Sachid, J. P. Llinas, Q. X. Wang, G. H. Ahn, G. Pitner, M. J. Kim, J. Bokor, C. M. Hu, H. S. P. Wong, and A. Javey, "MoS_2 transistors with 1-nanometer gate lengths," Science **354**(6308), 99–102 (2016).
[6]F. Wu, H. Tian, Y. Shen, Z. Hou, J. Ren, G. Y. Gou, Y. B. Sun, Y. Yang, and T. L. Ren, "Vertical MoS_2 transistors with sub-1-nm gate lengths," Nature **603**(7900), 259 (2022).
[7]L. Wang, J. S. Jie, Z. B. Shao, Q. Zhang, X. H. Zhang, Y. M. Wang, Z. Sun, and S. T. Lee, "MoS_2/Si heterojunction with vertically standing layered structure for ultrafast, high-detectivity, self-driven visible-near infrared photodetectors," Adv. Funct. Mater. **25**(19), 2910–2919 (2015).
[8]M. L. Tsai, S. H. Su, J. K. Chang, D. S. Tsai, C. H. Chen, C. I. Wu, L. J. Li, L. J. Chen, and J. H. He, "Monolayer MoS_2 heterojunction solar cells," ACS Nano **8**(8), 8317–8322 (2014).
[9]M. D. Losego, M. E. Grady, N. R. Sottos, D. G. Cahill, and P. V. Braun, "Effects of chemical bonding on heat transport across interfaces," Nat. Mater. **11**(6), 502–506 (2012).
[10]A. Giri and P. E. Hopkins, "A review of experimental and computational advances in thermal boundary conductance and nanoscale thermal transport across solid interfaces," Adv. Funct. Mater. **30**(8), 1903857 (2020).
[11]Y. Chalopin and S. Volz, "A microscopic formulation of the phonon transmission at the nanoscale," Appl. Phys. Lett. **103**(5), 051602 (2013).
[12]K. Gordiz and A. Henry, "Phonon transport at interfaces: Determining the correct modes of vibration," J. Appl. Phys. **119**(1), 015101 (2016).
[13]Y. G. Zhou and M. Hu, "Full quantification of frequency-dependent interfacial thermal conductance contributed by two- and three-phonon scattering processes from nonequilibrium molecular dynamics simulations," Phys. Rev. B **95**(11), 115313 (2017).
[14]Z. Cheng, R. Y. Li, X. X. Yan, G. Jernigan, J. J. Shi, M. E. Liao, N. J. Hines, C. A. Gadre, J. C. Idrobo, E. Lee, K. D. Hobart, M. S. Goorsky, X. Q. Pan, T. F. Luo, and S. Graham, "Experimental observation of localized interfacial phonon modes," Nat. Commun. **12**(1), 6901 (2021).
[15]Z. X. Lu, A. Vallabhaneni, B. Y. Cao, and X. L. Ruan, "Phonon branch-resolved electron-phonon coupling and the multitemperature model," Phys. Rev. B **98**(13), 134309 (2018).
[16]T. L. Feng, W. J. Yao, Z. Y. Wang, J. J. Shi, C. Li, B. Y. Cao, and X. L. Ruan, "Spectral analysis of nonequilibrium molecular dynamics: Spectral phonon temperature and local nonequilibrium in thin films and across interfaces," Phys. Rev. B **95**(19), 195202 (2017).

[17]T. L. Feng, Y. Zhong, J. J. Shi, and X. L. Ruan, "Unexpected high inelastic phonon transport across solid-solid interface: Modal nonequilibrium molecular dynamics simulations and Landauer analysis," Phys. Rev. B **99**(4), 045301 (2019).
[18]C. L. Tan, X. H. Cao, X. J. Wu, Q. Y. He, J. Yang, X. Zhang, J. Z. Chen, W. Zhao, S. K. Han, G. H. Nam, M. Sindoro, and H. Zhang, "Recent advances in ultrathin two-dimensional nanomaterials," Chem. Rev. **117**(9), 6225–6331 (2017).
[19]X. Cong, X. L. Liu, M. L. Lin, and P. H. Tan, "Application of Raman spectroscopy to probe fundamental properties of two-dimensional materials," npj 2D Mater. Appl. **4**(1), 13 (2020).
[20]S. Xu, N. Hunter, H. Zobeiri, H. Lin, W. Cheng, and X. Wang, "Distinct optical and acoustic phonon temperatures in nm-thick suspended WS_2: Direct differentiating via acoustic phonon thermal field invariant," Mater. Today Phys. **27**, 100816 (2022).
[21]R. S. Yan, J. R. Simpson, S. Bertolazzi, J. Brivio, M. Watson, X. F. Wu, A. Kis, T. F. Luo, A. R. H. Walker, and H. G. Xing, "Thermal conductivity of monolayer molybdenum disulfide obtained from temperature-dependent raman spectroscopy," ACS Nano **8**(1), 986–993 (2014).
[22]A. A. Balandin, S. Ghosh, W. Z. Bao, I. Calizo, D. Teweldebrhan, F. Miao, and C. N. Lau, "Superior thermal conductivity of single-layer graphene," Nano Lett. **8**(3), 902–907 (2008).
[23]R. D. Wang, S. Xu, Y. A. Yue, and X. W. Wang, "Thermal behavior of materials in laser-assisted extreme manufacturing: Raman-based novel characterization," Int. J. Extreme Manuf. **2**(3), 032004 (2020).
[24]R. D. Wang, H. Zobeiri, Y. S. Xie, X. W. Wang, X. Zhang, and Y. N. Yue, "Distinguishing optical and acoustic phonon temperatures and their energy coupling factor under photon excitation in nm 2D materials," Adv. Sci. **7**(13), 2000097 (2020).
[25]P. H. Tan, W. P. Han, W. J. Zhao, Z. H. Wu, K. Chang, H. Wang, Y. F. Wang, N. Bonini, N. Marzari, N. Pugno, G. Savini, A. Lombardo, and A. C. Ferrari, "The shear mode of multilayer graphene," Nat. Mater. **11**(4), 294–300 (2012).
[26]A. Taube, J. Judek, A. Lapiriska, and M. Zdrojek, "Temperature-dependent thermal properties of supported MoS_2 monolayers," ACS Appl. Mater. Interfaces **7**(9), 5061–5065 (2015).
[27]W. W. Cai, A. L. Moore, Y. W. Zhu, X. S. Li, S. S. Chen, L. Shi, and R. S. Ruoff, "Thermal transport in suspended and supported monolayer graphene grown by chemical vapor deposition," Nano Lett. **10**(5), 1645–1651 (2010).
[28]S. Karak, J. Bera, S. Paul, S. Sahu, and S. Saha, "Low thermal conductivity and interface thermal conductance in SnS_2," Phys. Rev. B **104**(19), 195304 (2021).
[29]I. Calizo, A. A. Balandin, W. Bao, F. Miao, and C. N. Lau, "Temperature dependence of the Raman spectra of graphene and graphene multilayers," Nano Lett. **7**(9), 2645–2649 (2007).
[30]B. Wei, Q. Y. Sun, C. Li, and J. W. Hong, "Phonon anharmonicity: A pertinent review of recent progress and perspective," Sci. China Phys. Mech. Astron. **64**(11), 117001 (2021).
[31]J. Liu, G. M. Choi, and D. G. Cahill, "Measurement of the anisotropic thermal conductivity of molybdenum disulfide by the time-resolved magneto-optic Kerr effect," J. Appl. Phys. **116**(23), 233107 (2014).
[32]P. Y. Yuan, C. Li, S. Xu, J. Liu, and X. W. Wang, "Interfacial thermal conductance between few to tens of layered-MoS_2 and c-Si: Effect of MoS_2 thickness," Acta Mater. **122**, 152–165 (2017).
[33]E. X. Pérez, *Design, Fabrication and Characterization of Porous Silicon Multilayer Optical Devices* (Universitat Rovira i Virgili, 2008).
[34]H. Zobeiri, N. Hunter, N. Van Velson, C. Deng, Q. Y. Zhang, and X. W. Wang, "Interfacial thermal resistance between nm-thick MoS_2 and quartz substrate: A critical revisit under phonon mode-wide thermal non-equilibrium," Nano Energy **89**, 106364 (2021).
[35]Z. Tian, S. Lee, and G. Chen, "Comprehensive review of heat transfer in thermoelectric materials and devices," Annu. Rev. Heat Transfer **17**, 425 (2014).
[36]X. N. Wang and A. Tabarraei, "Phonon thermal conductivity of monolayer MoS_2," Appl. Phys. Lett. **108**(19), 191905 (2016).
[37]M. Li, D. L. Cortie, J. X. Liu, D. H. Yu, S. M. K. N. Islam, L. L. Zhao, D. R. G. Mitchell, R. A. Mole, M. B. Cortie, S. X. Dou, and X. L. Wang, "Ultra-high thermoelectric performance in graphene incorporated Cu_2Se: Role of mismatching phonon modes," Nano Energy **53**, 993–1002 (2018).
[38]S. S. Yang, H. F. Song, Y. Peng, L. Zhao, Y. Z. Tong, F. Y. Kang, M. S. Xu, B. Sun, and X. Q. Wang, "Reduced thermal boundary conductance in GaN-based electronic devices introduced by metal bonding layer," Nano Res. **14**(10), 3616–3620 (2021).
[39]Z. Cheng, Y. R. Koh, H. Ahmad, R. J. Hu, J. J. Shi, M. E. Liao, Y. K. Wang, T. Y. Bai, R. Y. Li, E. Lee, E. A. Clinton, C. M. Matthews, Z. Engel, L. Yates, T. F. Luo, M. S. Goorsky, W. A. Doolittle, Z. T. Tian, P. E. Hopkins, and S. Graham, "Thermal conductance across harmonic-matched epitaxial Al-sapphire heterointerfaces," Commun. Phys. **3**(1), 115 (2020).
[40]B. Qiu and X. L. Ruan, "Reduction of spectral phonon relaxation times from suspended to supported graphene," Appl. Phys. Lett. **100**(19), 193101 (2012).
[41]J. H. Seol, I. Jo, A. L. Moore, L. Lindsay, Z. H. Aitken, M. T. Pettes, X. S. Li, Z. Yao, R. Huang, D. Broido, N. Mingo, R. S. Ruoff, and L. Shi, "Two-dimensional phonon transport in supported graphene," Science **328**(5975), 213–216 (2010).